Theoretical Analysis of Bioassays Based on Microlaser Ensembles

Weishu Wu and Xudong Fan

***Abstract*—We present a bioassay platform based on microlaser ensembles, offering a sensitive assay method with a high dynamic range. In this platform, microlasers are functionalized to capture analytes. The captured analytes introduce quenchers, thus increasing microlasers' lasing thresholds and even turning off microlaser emission. We develop a theoretical model to count the number of quenchers and hence the number of captured analytes for microlasers by measuring their lasing thresholds. A statistical model is established to link the distribution of captured analytes to the lasing fraction of microlasers. Fundamentally different from digital ELISA, in which a microunit (such as a microbead) saturates when more than one analyte is present, the microlaser-based method can perform multiple quantized signal readouts by scanning the external pump across the lasing threshold. Therefore, this platform does not require the average number of analytes per microlaser be much lower than one, thus achieving a higher dynamic range. The detection limit and the factors that may affect the detection limit are also discussed.**

***Index Terms*—Bioassays, microlasers, laser quenching, microlaser ensemble.**

NOMENCLATURE

$n_{1,Gain}$	Density of the laser gain molecules in the excited state.
$n_{T,Gain}$	Total density of the laser gain molecules in the microlaser.
n_q	Quencher density at the lasing wavelength.
$s_{e,Gain}$	Emission cross section of the laser gain molecules at the lasing wavelength.
$s_{a,Gain}$	Absorption cross section of the laser gain molecules at the lasing wavelength.
$s_{a,q}$	Quencher's absorption cross section at the lasing wavelength.
L	Intrinsic single-trip laser cavity loss in the absence of quenchers.
k	Analyte number inside a microlaser.
g_0	$\frac{n_{1,Gain}}{n_{T,Gain}}$ at the lasing threshold for an unquenched microlaser.
g	$\frac{n_{1,Gain}}{n_{T,Gain}}$ at the lasing threshold for a quenched microlaser.
t_{Gain}	Lifetime of the gain molecules.
t_{Fl}	Lifetime of the fluorophores.
N_q	Number of quenchers inside a microlaser.
S	Number of the substrate molecules during reaction.
S_0	Initial number of the substrate molecule.
C_2	Reaction constant for enzyme-substrate reaction.
T	Reaction time for enzyme-substrate reaction.
I_t	Lasing threshold in units of flux for the microlaser.
I_{th}^{exp}	Experimentally measured pump intensity (or flux).
$R_{Collect}$	Photon collection efficiency of the photodetector in experiments.
R_{Sens}	Sensitivity ratio between the microlaser quenching and fluorescence-based methods.
α	Absorption parameter for the non-linearity of optical absorption for the fluorescence-based biosensor.
V_0	Volume of the microlaser cavity.
$I_{sat,Gain}$	Saturation photon flux of the gain molecule.
$I_{sat,Fl}$	Saturation flux of the fluorophore.
C	Concentration of the analytes in the liquid sample.
k_i	Analyte number on the $\mathrm{i_{th}}$ microlaser.
m_c	Mean of the analyte molecule number distribution.
s_c	Standard deviation of the analyte molecule number distribution.
μ_c^{Fl}	Mean of the signal intensity distribution for the fluorescence-based method.
σ_c^{Fl}	Standard deviation of the signal intensity distribution for the fluorescence-based method.
μ_c^{th}	Mean of the signal intensity distribution for the microlaser quenching method.
σ_c^{th}	Standard deviation of the signal intensity distribution for the microlaser quenching method.
P_{Fl}	Total photon emission rate in the fluorescence-based method.
P_{th}^{exp}	Experimentally measured photon emission rate in the fluorescence-based method.
P_{th}	Pump photon absorption rate at the lasing threshold.
$N_{1,Fl}$	Number of fluorophores in the excited state.
P_{th}^{enzyme}	Sensing signal for the enzyme labelling method.
Q_e	Quantum yield of the fluorophore.
$I_{p,Fl}$	Flux of the excitation light in the fluorescence-based method.
$\sigma_{a,Fl}$	Absorption cross section of the fluorophore.
S_{Fl}	Emitted photon rate change in response to the change of the analyte number.

Received 17 October 2025; revised 12 January 2026 and 10 February 2026; accepted 11 February 2026. Date of publication 17 February 2026; date of current version 2 March 2026. *(Corresponding author: Xudong Fan.)*

The authors are with the Department of Biomedical Engineering, University of Michigan, Ann Arbor, MI 48109 USA, also with the Center for Wireless Integrated MicroSensing and Systems (WIMS2), University of Michigan, Ann Arbor, MI 48109 USA, and also with the Max Harry Weil Institute for Critical Care Research and Innovation, University of Michigan, Ann Arbor, MI 48109 USA (e-mail: xsfan@umich.edu).

Color versions of one or more figures in this article are available at https://doi.org/10.1109/JSTQE.2026.3665681.

Digital Object Identifier 10.1109/JSTQE.2026.3665681

$\Sigma_{a,Gain}$ Total absorption cross section of the gain molecules inside the microlaser at the pump wavelength.

β Absorption parameter for the non-linearity of optical absorption for the microlaser quenching method.

I. Introduction

BIOASSAYS are critical for biological research and clinical diagnosis. Their working principle is to convert the presence of molecules of interest (analytes) into measurable quantities, such as luminescence intensities or spectral shifts. Among these methods, enzyme-linked immunosorbent assay (ELISA) has been proven to be a sensitive and highly specific platform [1], [2]. In ELISA, capture antibodies are immobilized on a reaction surface and bind to analytes. Detection antibodies tagged with enzymes then bind to the captured analytes. Upon addition of a suitable substrate, the enzyme–substrate reaction generates light signals (i.e., chemiluminescence) [3], [4]. Alternatively, substrate-free detection schemes employ tagging detection antibodies with fluorescent labels [5] (i.e., dyes [6] and quantum dots [7], [8], [9]) to generate light signals (i.e., fluorescence). The light signals are measured to quantify the analyte concentration. In conventional bioassays, since the measured signal varies continuously with the analyte concentration, it is called analog detection [10], [11], [12], [13], [14].

Recently, digital ELISA was developed to improve sensitivity and detection limit [15], [16], [17], [18], [19], [20], [21], [22]. This approach allocates analytes to an ensemble of microunits or microcompartments (such as microbeads) and then counts the fraction of these microunits that emit light. Poisson statistics are subsequently applied to the microunits with the assumption that the average analyte number per microbead is far below one [23]. When the analyte concentration is high, however, the above assumption breaks down, which limits the applications of digital ELISA in high-analyte-concentration scenarios. Some strategies have been explored, including stitching the digital detection calibration curve with the analog detection calibration curve [16], [22] or extrapolating the calibration curve beyond the single-analyte assumption [24]. However, stitching causes discontinuity in digital and analog calibration curves due to the two completely different methods used to obtain the digital and analog sensing signals [24]. A unified method with a high dynamic range to cover both the lower and the upper ends of the analyte concentration without any artificially introduced digital-to-analog transition is highly desirable.

In this work, we propose and analyze a bioassay platform using a microlaser ensemble, where a microlaser is used as the microunit. We first show that the lasing threshold of a microlaser is modulated by the number of analytes it captures. We then present a detailed theoretical model to describe the quantitative relation between the lasing threshold increase in a microlaser and the number of analytes it captures. Subsequently, a statistical model is proposed to generalize the model from a single microlaser to an ensemble of microlasers, allowing higher repeatability of the system. We show that in this detection scheme, by measuring the increase of the lasing threshold, our microunit (i.e., microlaser) can differentiate the number of analytes. This helps our system to overcome the constraining assumption of digital ELISA that the average analyte number needs to be much smaller than one. As a result, our system shows a high dynamic range, while still achieving a low detection limit.

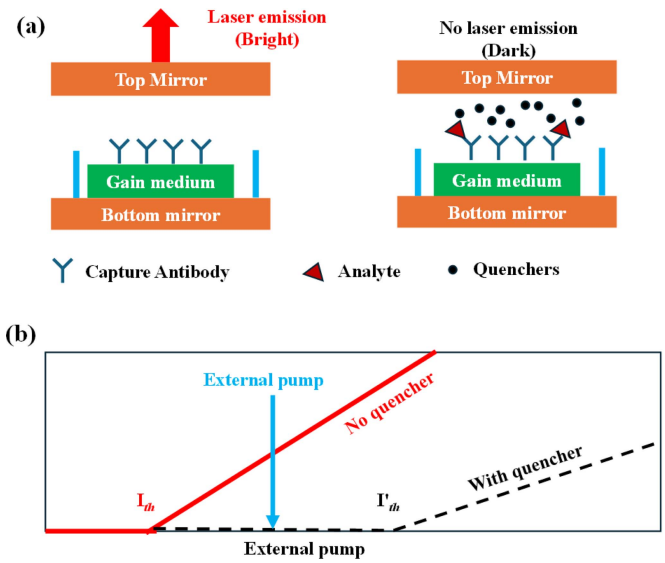

Fig. 1. (a) A sketch of the single microlaser model. The top and bottom mirrors form a Fabry-Perot cavity. Capture antibodies (biorecognition molecules) are coated on the surface of the gain medium and bind to molecules of interest (analytes). After binding, quenchers are produced inside the cavity, causing an increase in the lasing threshold of the microlaser. As a result, the initial "bright" microlaser that has laser emission (meaning that the external pump is higher than the lasing threshold) is quenched and becomes a "dark" microlaser (meaning that the same external pump is lower than the new lasing threshold) (b) Schematic showing the relationship between the external pump and the lasing threshold values before and after the presence of the quenchers. The presence of the quenchers turns the bright microlaser into a dark microlaser.

II. Single Microlaser Assay Model

We first consider a bioassay model using a single microlaser as shown in Fig. 1(a). For a laser to operate, we need (1) a gain medium (such as dyes and semiconductor materials), (2) optical feedback provided by an optical cavity (such as a Fabry-Perot cavity or a ring resonator), and (3) an external pump (such as optical pump and electrical pump). Laser emission is achieved when the external pump is above the lasing threshold.

The inside of the laser cavity can be coated or filled (functionalized) with biorecognition molecules such as capture antibodies. These capture antibodies (or other biorecognition molecules) bind to analytes specifically. Without losing generality, the surface of the gain medium inside the laser cavity is coated with capture antibodies as shown in Fig. 1(a). Then, the test sample is added into the laser cavity, and analyte molecules are captured. A labelling step is performed, where light-absorbing molecules (quenchers) are introduced into the cavity to tag the captured analytes. The presence of these quenchers increases light absorption in the cavity and hence the lasing threshold. Fig. 1(b) illustrates this increase in lasing threshold, and how this increase can be observed with a given external pump. Initially, when no quencher is present in the laser

cavity, the external pump is larger than the lasing threshold and the laser emission can be observed ("bright" microlaser). After adding quenchers into the microlaser, the increased lasing threshold surpasses the external pump, the laser emission is turned off ("dark" microlaser). In this work, we focus on using the increase in the lasing threshold of a microlaser to recover the number of analytes in the laser cavity.

Here we use dye as the gain medium to give a quantitative description of the lasing threshold change in a microlaser with respect to the number of captured analytes. The overall derivations can easily be extended to other lasers, such as semiconductor lasers. The definitions of all variables can be found in the Nomenclature. For this microlaser to lase, the following condition should be met [25], [26], [27], [28]:

$$n_{1,Gain}\sigma_{e,Gain} \geq (n_{T,Gain} - n_{1,Gain})\,\sigma_{a,Gain} + L + n_q\sigma_{a,q}, \tag{1.1}$$

where $n_{T,Gain}$ is the total density of the laser gain molecules (i.e., dyes) in the microlaser. $n_{1,Gain}$ is the density of the laser gain molecules in the excited state. $\sigma_{e,Gain}$ and $\sigma_{a,Gain}$ are the emission and absorption cross section of the laser gain molecule at the lasing wavelength, respectively. L is the intrinsic single-trip laser cavity loss in the absence of quenchers. n_q and $\sigma_{a,q}$ are the quencher's density and the absorption cross section at the lasing wavelength, respectively. In (1.1), the presence of quenchers leads to an increased lasing threshold. By flipping the sign of the term $\sigma_{a,q}$ (that is, replacing $\sigma_{a,q}$ with σ_e, the emission cross section of a light-emitting molecule) the model can be used for the case where light-emitting molecules are used to decrease the lasing threshold. The detailed equations that analyze the lasing threshold change can be found in [25]. However, (1.1) provides better insight into the microlaser lasing threshold behavior. Rearranging (1.1), we have:

$$\frac{n_{1,Gain}}{n_{T,Gain}} \geq \frac{\sigma_{a,Gain}}{\sigma_{e,Gain}+\sigma_{a,Gain}}\left[1+\frac{L}{n_{T,Gain}\sigma_{a,Gain}}\right] + \frac{n_q\sigma_{a,q}}{n_{T,Gain}\left(\sigma_{e,Gain}+\sigma_{a,Gain}\right)}, \tag{1.2}$$

which can be approximated as:

$$\frac{n_{1,Gain}}{n_{T,Gain}} \geq \frac{\sigma_{a,Gain}}{\sigma_{e,Gain}}\left[1+\frac{L}{n_{T,Gain}\sigma_{a,Gain}}\right] + \frac{n_q\sigma_{a,q}}{n_{T,Gain}\sigma_{e,Gain}}, \tag{1.3}$$

because $s_{a,Gain}$ ($\sim 10^{-18}$ cm^2 for dyes) is usually much smaller than $s_{e,Gain}$ ($\sim 10^{-16}$ cm^2 for dyes). Therefore, at the lasing threshold, (1.3) becomes:

$$\gamma = \frac{n_{1,Gain}}{n_{T,Gain}} = \gamma_0 + Xn_q, \tag{1.4}$$

where γ_0 and X are:

$$\gamma_0 = \frac{\sigma_{a,Gain}}{\sigma_{e,Gain}}\left(1+\frac{L}{n_{T,Gain}\sigma_{a,Gain}}\right), \tag{1.5}$$

$$X = \frac{\sigma_{a,q}}{n_{T,Gain}\sigma_{e,Gain}}. \tag{1.6}$$

Equation (1.4) states that for a microlaser in the absence of quenchers, we have $\gamma\ (n_q = 0) = \gamma_0$, which corresponds to $\frac{n_{1,Gain}}{n_{T,Gain}}$ at the lasing threshold for an unquenched microlaser. γ increases linearly with respect to the quencher density n_q, that is, in the presence of quenchers, the microlaser needs to receive a higher pump intensity (or flux) and hence a higher $\frac{n_{1,Gain}}{n_{T,Gain}}$ to reach the lasing threshold.

Without losing generality, we use a four-energy-level laser system model, which is suitable for dye lasers. At the lasing threshold, we have:

$$\gamma = \frac{\frac{I_{th}}{I_{sat,Gain}}}{\frac{I_{th}}{I_{sat,Gain}}+1} = \frac{\widetilde{I_{th}}}{\widetilde{I_{th}}+1}, \tag{1.7}$$

where I_{th} is the lasing threshold in a unit of flux (Jm^{-2}s^{-1}) for the laser. $I_{sat,Gain} = (s_{a,Gain}t_{Gain})^{-1}$ is the saturation flux of the gain molecule, where $s_{a,Gain}$ and t_{Gain} are the absorption cross section and the lifetime of the gain molecule, respectively. $\widetilde{I_{th}}$ is the dimensionless normalized lasing threshold to simplify the expression. This increase in the lasing threshold can be measured as pump intensity (or flux) I_{th}^{exp} in experiments. Let R_{eff} be an efficiency that considers the difference between the pump intensity measured experimentally (I_{th}^{exp}) and the actual pump intensity seen by the gain molecules, we have:

$$\widetilde{I_{th}} = R_{eff}\frac{I_{th}^{exp}}{I_{sat,Gain}} = \frac{I_{th}^{exp}}{I_{norm}}. \tag{1.8}$$

A. Quenchers vs. Captured Analytes

From the derivations above, it is clear that the lasing threshold is directly related to the number of quenchers present in the microlaser. Below, we will discuss the relationship between the number of quenchers and the number of analytes captured by the microlaser. There are two major methods of introducing quenchers into the microlasers. The first method is direct labelling, where quenchers are conjugated onto antibodies. These antibodies then bind to the captured analytes specifically. In this method, the ratio between the number of quenchers and the analyte number is constant. The second method is enzyme labelling. In this method, enzymes (which do not directly absorb light) are conjugated with the antibodies, which then bind to the captured analytes. Subsequently, substrate molecules are added to the microlasers. Enzymes catalyze the substrate molecules to produce quenchers. In this process, the quencher-analyte ratio is no longer constant.

B. Direct Labelling

We start from the relation between quenchers and analytes:

$$n_q = \frac{1}{M}\,k, \tag{1.9}$$

where M is the analyte-quencher ratio, and k is the number of analytes captured in a microlaser. Note that the above equation is linear and works when the number of quenchers is low. For a

high number of quenchers, we have:

$$n_q = \frac{1}{M}\frac{k}{1+\alpha k}, \tag{1.10}$$

where α is a parameter that accounts for the saturation effect of optical absorption at a high quencher number. At a low quencher number, (1.10) becomes (1.9), since α is small. Using (1.4), we have the form of the relation between the lasing threshold and the analyte number:

$$\gamma = \frac{n_{1,Gain}}{n_{T,Gain}} = \gamma_0 + \frac{X}{M}\frac{k}{1+\alpha k}, \tag{1.11}$$

This gives us the relation:

$$\begin{aligned} k &= \frac{(\gamma - \gamma_0)\frac{M}{X}}{1 - \alpha(\gamma - \gamma_0)\frac{M}{X}} \\ &= \frac{\left(\frac{\frac{I_{th}^{exp}}{I_{norm}} - \frac{I_0}{I_{norm}}}{\left(\frac{I_{th}^{exp}}{I_{norm}}+1\right)\left(\frac{I_0}{I_{norm}}+1\right)}\right)\frac{M}{X}}{1 - \alpha\left(\frac{\frac{I_{th}^{exp}}{I_{norm}} - \frac{I_0}{I_{norm}}}{\left(\frac{I_{th}^{exp}}{I_{norm}}+1\right)\left(\frac{I_0}{I_{norm}}+1\right)}\right)\frac{M}{X}}, \end{aligned} \tag{1.12}$$

where all variables are defined in the previous equations. I_0 is the lasing threshold of the microlaser measured experimentally when there is no analyte (or quencher) present. It is connected to γ_0 through:

$$\gamma_0 = \frac{\widetilde{I_0}}{\widetilde{I_0}+1} = \frac{\frac{I_0}{I_{norm}}}{\frac{I_0}{I_{norm}}+1}. \tag{1.13}$$

C. Enzyme Labelling

Quenchers can also be produced by enzyme-catalyzed reactions. First, we study the relation between the number of quenchers, n_q, and the analyte number, k, associated with a microlaser, and establish a relation similar to (1.10). In enzyme labelling, the ratio between the number of enzymes and the number of analytes is constant, while quenchers are produced in a subsequent enzyme-catalyzed reaction. We assume that the number of enzymes inside a microlaser, D, has a simple form of $D = C_1\ k$, where C_1 is the enzyme-to-analyte ratio. In a microlaser model with limited substrate molecules for reaction, let S be the total number of substrate molecules during the reaction, S_0 be the initial number of substrate molecules, C_2 be a reaction constant, and T be the reaction time, we have:

$$\frac{dS}{dt} = -C_2\frac{D}{V_0}S = -C_2C_1\frac{kS}{V_0}, \tag{1.14}$$

$$n_q = \frac{N_q}{V_0} = \frac{S_0 - S(T)}{V_0} = \frac{S_0}{V_0}\left(1 - \frac{1}{e^{C_1C_2kT/V_0}}\right), \tag{1.15}$$

where V_0 is the volume of the microlaser cavity. Equation (1.14) states that in the enzyme-catalyzed reaction, where the substrate molecules are consumed, the reaction rate is proportional to the enzyme number and the substrate molecule number. Equation (1.15) states that the number of quenchers is proportional to the product of the reaction, which can be expressed as the total number of substrate molecules consumed. When C_1C_2kT/V_0 is small, n_q is approximately linear with respect to k. However, when k and T become higher, this linear relationship starts to deviate. From (1.15), we can establish the relation between n_q and k for a fixed reaction time:

$$n_q = A\left(1 - \frac{1}{e^{Ek}}\right), \tag{1.16}$$

where A and E are two constants. Substituting (1.16) into (1.4), we have:

$$\gamma = \gamma_0 + XA\left(1 - \frac{1}{e^{Ek}}\right), \tag{1.17}$$

which connects the fraction of the gain molecules in the excited state at the lasing threshold (i.e., γ) to the number of analytes captured by the microlaser.

Next, we connect the analyte number on a microlaser with the experimentally measured lasing threshold of a microlaser I_{th}^{exp}. Considering the boundary condition that states that when the analyte number on the microlaser is high, the microlaser breaks down ($I_{th} \to \infty$), we have:

$$lim_{k\to\infty}(\gamma) = 1, \tag{1.18}$$

which leads to a simplified form of (1.17), i.e.,:

$$\gamma = \gamma_0 + (1-\gamma_0)\left(1 - \frac{1}{e^{Ek}}\right). \tag{1.19}$$

γ_0 and its relationship with I_0 are defined in (1.13). The expression of the experimentally measured lasing threshold of a microlaser with respect to the analyte number inside the microlaser is:

$$I_{th}^{exp} - I_0 = (I_{norm} + I_0)\ (e^{Ek} - 1), \tag{1.20}$$

which in turn leads to:

$$k = \frac{ln\left(\frac{I_{th}^{exp}+I_{norm}}{I_0+I_{norm}}\right)}{E}. \tag{1.21}$$

Equation (1.21) shows how to obtain the analyte number associated with a microlaser using the experimentally measured lasing threshold. I_{norm} and E can be obtained using function fittings from experimental data.

In summary, through (1.12) and (1.21), the number of analytes captured by the microlaser, k, is directly connected to the lasing threshold of the microlaser, I_{th}^{exp}. The constant, I_{norm}, is defined by (1.8), but in practice, it can be obtained using function fittings from experimental data. So far, we have established the fundamental theory to perform bioassays using single microlasers. From (1.12) and (1.21), one can establish a calibration curve that connects the calculated k value with the test sample concentration C.

III. Microlaser Ensemble Assay Model

In the previous section, we established the theory for using single microlasers for bioassays. In this section, we generalize the results from single microlasers to a microlaser ensemble as illustrated in Fig. 2(a). A microlaser ensemble is defined as a large quantity ($>10^3$) of identical and optically isolated

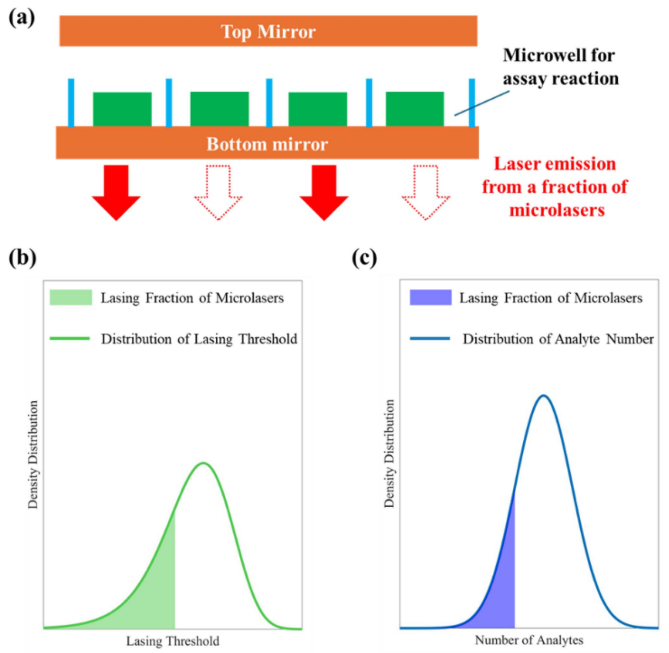

Fig. 2. (a) Illustration of an ensemble of microlasers used for measuring analyte distribution after capturing analytes. When the ensemble is pumped at a constant pump intensity, not all microlasers lase due to a distribution of analytes, which leads to a distribution of lasing thresholds. (b) Lasing threshold distribution in a microlaser ensemble. The green-shaded area represents the lasing fraction of the ensemble when pumped at a specific pump intensity. (c) Distribution of analytes in the same ensemble as in (b). The blue-shaded area represents the fraction of analytes that corresponds to the bright microlasers (lasing fraction) in (b), showing that pumping at one pump intensity is equivalent to probing the number of analytes lower than a specific value. Therefore, by scanning the pump intensity in (b), we can map the analyte distribution in (c).

microlasers. During an assay, the microlaser ensemble interacts with the liquid sample containing analytes. In the incubation step, analytes bind to each microlaser in the same manner as discussed in the previous section. The binding process leads to a distribution of analytes in the microlaser ensemble. Using the distribution measurements from the microlaser ensemble (such as the mean of analyte number captured by microlasers) can effectively reduce the variance in experiments caused by the fluctuation in the analytes captured by a microlaser (from the randomness of analyte binding) and the inherent lasing threshold variation (from the microlaser fabrication process) from a single microlaser.

We use a few assumptions to build a model to describe the distribution of analytes in the ensemble. In the analyte binding step, the microlasers in the ensemble are identical. Furthermore, we assume that the occurrence of binding events is independent. From these, the distribution of analytes in the microlasers can be described by a Poisson distribution. In actual assays, the analyte-to-microlaser ratio often exceeds 1000 (for example, a test sample with a volume of 100 μL and concentration of 20 fM interacting with a microlaser ensemble of 10^3 microlasers). For a Poisson distribution with a large mean value, we approximate it with a Gaussian distribution. In the Discussion and Conclusion section, we will present more advantages of using a Gaussian distribution.

For microlaser j in the ensemble, if k_j is the number of analytes captured by this microlaser, we have:

$$k_j \sim \text{Gaussian}\left(\mu_c, \sigma_c\right), \tag{2.1}$$

where μ_c and σ_c are the mean and the standard deviation of the distribution of analytes. They e dependent on C, the concentration of the analytes in the liquid sample. Below, we present a method of measuring the analyte number distribution on a microlaser ensemble by measuring its lasing threshold distribution.

Under a fixed pump intensity, $I_{pump}^{exp}(i)$, we count the number of lasing microlasers ("bright") to calculate the lasing fraction in the microlaser ensemble. These lasing microlasers all have lasing thresholds smaller than or equal to the pump intensity, as illustrated in Fig. 2(b). Therefore, by changing the pump intensity, we probe the lasing threshold distribution in the microlaser ensemble. From the conclusion in the previous section, probing the lasing threshold distribution is equivalent to probing the distribution of the analytes in the microlaser ensemble, which is illustrated in Fig. 2(c). Mathematically, it can be stated as the lasing fraction and the pump intensity follow the equation below:

$$Lf(i) = \phi_{cumu}\left(k_i; \mu_c, \sigma_c\right). \tag{2.2}$$

ϕ_{cumu} stands for the standard Gaussian cumulative distribution function. As discussed in the previous section, at this pump intensity value $I_{pump}^{exp}(i)$, the microlasers with fewer than k_i analytes have laser emission ("bright" microlasers) and those with more than k_i analytes do not have laser emission ("dark" microlasers). For direct labelling, we have:

$$k_i = \frac{\left(\frac{\frac{I_{pump}^{exp}(i)}{I_{norm}} - \frac{I_0}{I_{norm}}}{\left(\frac{I_{pump}^{exp}(i)}{I_{norm}}+1\right)\left(\frac{I_0}{I_{norm}}+1\right)}\right)\frac{M}{X}}{1 - \alpha\left(\frac{\frac{I_{pump}^{exp}(i)}{I_{norm}} - \frac{I_0}{I_{norm}}}{\left(\frac{I_{pump}^{exp}(i)}{I_{norm}}+1\right)\left(\frac{I_0}{I_{norm}}+1\right)}\right)\frac{M}{X}}, \tag{2.3}$$

whereas for enzyme labelling, we have:

$$k_i = \frac{ln\left(\frac{I_{pump}^{exp}(i)+I_{norm}}{I_0+I_{norm}}\right)}{E}, \tag{2.4}$$

where $I_{pump}^{exp}(i)$ denotes a specific pump intensity. By using multiple pump intensities, we can obtain a set of data, [($Lf(i)$, $I_{pump}^{exp}(i)$)], which can be used to fit the standard Gaussian cumulative distribution and obtain μ_c and σ_c. Finally, by using the one-to-one correspondence between the distribution of analytes μ_c (and σ_c) and the analyte concentration, C, in the liquid solution, we can obtain the analyte concentration. This correspondence between μ_c (and σ_c) of a microlaser ensemble and the analyte concentration, C, can be established by a calibration step experimentally.

In Fig. 3, we show a comparison of our method with digital ELISA. In digital ELISA, a positive signal indicates that one and only one analyte is present in the microunit. The microunit is saturated when more than one analyte is in it, as illustrated in Fig. 3(a). For an ensemble of microunits, the average number of analytes per microunit must be much lower than one so

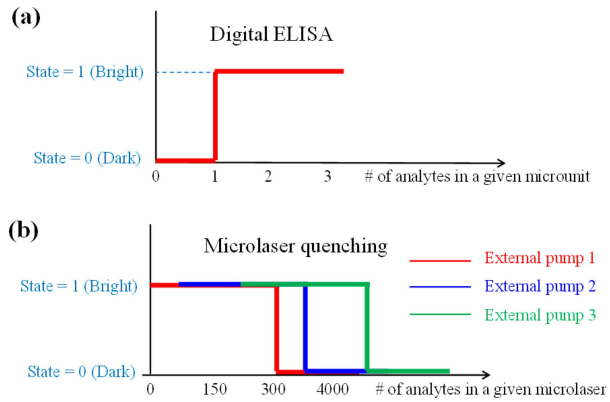

Fig. 3. (a) Response function of a microunit for digital ELISA. It is saturated when there is more than one analyte present, leading to a limited dynamic range. (b) Response functions of a microlaser. By changing the external pump, the microlaser can be tuned to differentiate different numbers of analytes, which allows the microlaser-based method to have a much higher dynamic range.

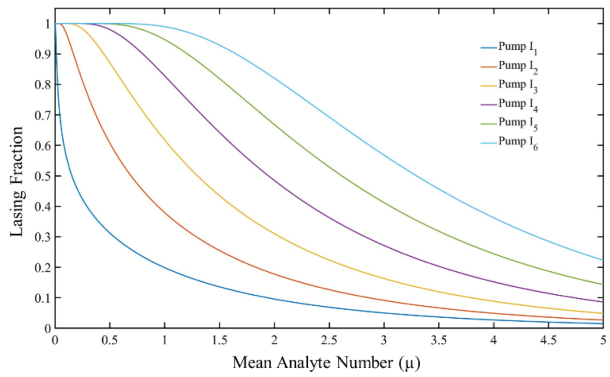

Fig. 4. A plot showing the change of lasing fractions of microlaser ensembles with respect to the mean analyte number on the microlaser ensembles at fixed external pumps. Pump $I_1 = 25\ \mu J/\text{mm}^2$, Pump $I_2 = 50\ \mu J/\text{mm}^2$, Pump $I_3 = 100\ \mu J/\text{mm}^2$, Pump $I_4 = 200\ \mu J/\text{mm}^2$, $Pump\ I_5 = 400\ \mu J/\text{mm}^2$, Pump $I_6 = 800\ \mu J/\text{mm}^2$. We set the constant values $I_0 = 20.0\ \mu J/\text{mm}^2$, $I_{norm} = 10.0\ \mu J/\text{mm}^2$, these are the values that are comparable to our experiment observations in [29]. Unlike conventional sensors, our microlaser-based method has multiple calibration curves. The sensitivity, i.e., the slope of the curve, of the same microlaser ensemble can be tuned by the external pump.

that the contribution of the saturated microunits is insignificant. In contrast, for the microlaser-based method, we can perform multiple quantized signal readouts by scanning across the lasing threshold, which can be easily done by tuning the external pump, as schematically illustrated in Fig. 3(b) and mathematically described in (2.3) and (2.4). Therefore, our method lifts the constraint that the average number of analytes per microunit should be much lower than one, thus achieving a higher dynamic range. Practically, digital ELISA usually uses 10^5-10^6 microunits to ensure that the number of microunits is far higher than the number of analytes to be analyzed. In contrast, in the microlaser-based method, the number of microlasers can be only 10^3-10^4, as shown in our experiments published elsewhere [29].

In Fig. 4, we show, as an example, a simulated plot of lasing fraction as a function of the mean analyte number on microlaser ensembles when quenchers are produced by enzyme-catalyzed reactions. Here, the mean analyte number can be used for concentration recovery in the test sample. Notice that an experimental calibration curve is needed to establish the relation between the mean analyte number and the analyte concentration. This relation depends on multiple experimental factors such as the affinity between the capture antibodies and analytes, incubation time in the binding process, and surface density of capture antibodies on microlasers. This is beyond the scope of this work. For an experimentally established calibration relation between the mean analyte number and lasing fractions, refer to [29]. From (2.4), we can obtain a group of functions, where each function shows the lasing fraction of the microlaser ensemble changes with the analyte concentration in the test sample when the external pump is set at a specific value. In our simulation, the values of the external pumps are set from 25 μJ/mm^2 to 800 μJ/mm^2. Other parameters are set as: $I_0 = 20.0\ \mu$J/mm^2, $I_{norm} = 10.0\ \mu$J/mm^2, and $E = 1$. The distributions of analytes are approximated by Gaussian distributions (with an extra condition where $\sigma^2 = \mu$). Unlike conventional biosensors, where there is only one calibration curve (showing the relationship between the sensor signal and the analyte concentration), our platform offers multiple, nonlinearly related calibration curves. These curves cover a broad range of analyte concentration and increase the dynamic range of the platform.

IV. Sensitivity Analysis

In the previous sections, we investigated the assay mechanism based on microlaser ensembles. By measuring the change of the lasing threshold distribution of microlasers, one can calculate the distribution of analytes on the microlasers, which can then be used to recover the analyte concentration in the test sample. While traditional fluorescence-based methods can also be used to perform a similar measurement strategy, we will show that the sensitivity of the fluorescence-based methods is orders of magnitude smaller than our microlaser-based method.

A. Sensitivity of Fluorescence-Based Sensors in Detecting Analyte Distribution

To compare the sensitivity of the microlaser-based methods with conventional fluorescence-based methods (tagging analytes with dyes, quantum dots, and engineered fluorescent molecules, *etc.*), we calculate the signal change for each sensor per captured analyte. For the fluorescence-based sensor, the fluorescence intensity is used to quantify the analyte. We assume that each analyte has only one fluorophore attached to it. When k analytes are attached to the sensor, the signal intensity, represented by the total photon emission rate P_{Fl}, is:

$$P_{Fl} = \frac{Q_e}{\tau_{Fl}} N_{1,Fl}, \tag{3.1}$$

where $N_{1,Fl}$ is the number of fluorophores in the excited state. t_{FL} and Q_e are the lifetime and quantum yield of the fluorophore, respectively. $N_{1,Fl}$ is related to the total number of fluorophores $N_{T,\ Fl}$ $(= k)$ by:

$$\begin{aligned} &I_{p,Fl}\sigma_{a,Fl}\left(N_{T,\ Fl} - N_{1,\ Fl}\right) \\ &= I_{p,FL}\,\sigma_{a,Fl}\ (k - N_{1,\ Fl}) = \frac{N_{1,\ Fl}}{\tau_{Fl}}, \end{aligned} \tag{3.2}$$

where $I_{p,Fl}$ is the flux of the excitation light and $s_{a,Fl}$ is the absorption cross section of the fluorophore. Combining (3.1) and (3.2), we have:

$$P_{Fl} = \frac{Q_e}{\tau_{Fl}} \frac{I_{p,Fl}\sigma_{a,Fl}\tau_{Fl}}{1 + I_{p,Fl}\sigma_{a,Fl}\tau_{Fl}} k = \frac{Q_e}{\tau_{Fl}} \frac{\frac{I_{p,FL}}{I_{sat,Fl}}}{1 + \frac{I_{p,FL}}{I_{sat,Fl}}} k, \quad (3.3)$$

where $I_{sat,Fl} = (s_{a,Fl}t_{Fl})^{-1}$ is the saturation flux of the fluorophore. Practically, only a portion of the emitted photons can be collected. Therefore,

$$P_{Fl}^{Exp} = R_{Collect} \frac{Q_e}{\tau_{Fl}} \frac{\frac{I_{p,Fl}}{I_{sat,Fl}}}{1 + \frac{I_{p,Fl}}{I_{sat,Fl}}} k, \quad (3.4)$$

where P_{Fl}^{Exp} is experimentally measured photon emission rate and $R_{Collect}$ is the photon collection efficiency.

The sensitivity of fluorescence-based methods, S_{Fl}, is defined as the emitted photon rate chge in response to the change of the analyte number, i.e.,

$$S_{Fl} = \frac{dP_{Fl}^{Exp}}{dk} = R_{Collect} \frac{Q_e}{\tau_{Fl}} \frac{\frac{I_{p,Fl}}{I_{sat,Fl}}}{1 + \frac{I_{p,Fl}}{I_{sat,Fl}}}, \quad (3.5)$$

which gives the photon emission rate change when the analyte number changes from k to $k+1$.

B. Sensitivity of Microlaser-Based Sensors in Detecting Analyte Distribution

Now we calculate the sensitivity for our microlaser-based method. The sensor signals from microlaser-based sensors are lasing thresholds of the microlasers. For comparison purposes, we assume that each analyte has only one quencher molecule associated with it. This is a fair comparison to the fluorescence-based method discussed previously, where each analyte has only one fluorophore attached to it. This is different from the model where multiple quenchers can be generated for each analyte. According to (1.7), the lasing threshold of the microlaser, I_{th}, can be expressed as

$$I_{th} = I_{sat,Gain} \frac{\gamma}{1 - \gamma}. \quad (3.6)$$

where $I_{sat,Gain}$ is the saturation photon flux of the gain molecule and g is given by (1.4)

$$\gamma = \gamma_0 + X\, n_q = \gamma_0 + X \frac{k}{V_0}, \quad (3.7)$$

where V_0 is the microlaser volume that converts the number of quenchers (or analytes) into the density of quenchers (or analytes).

The sensitivity of microlaser-based detection is defined as the lasing threshold change in response to the change of the analyte number from k to $k+1$, i.e.,

$$\frac{dI_{th}}{dk} = I_{sat,Gain} \left(\frac{1}{(1 - \gamma)^2} \right) \frac{X}{V_0}. \quad (3.8)$$

To further simplify (3.8), without losing generality, we assume that $s_{a,q} = s_{e,Gain}$. As a result, (3.8) becomes:

$$\frac{dI_{th}}{dk} = \frac{I_{sat,Gain}}{V_0 n_T} \frac{1}{\left(1 - \gamma_0 - \frac{k}{V_0 n_{T,Gain}}\right)^2}. \quad (3.9)$$

Note that the sensitivity defined in (3.9) has a unit of $\mathrm{m}^{-2}\mathrm{s}^{-1}$ (excitation photon flux), which is different from S_{Fl}, which carries a unit of s^{-1}. To make a direct comparison, we use the following equations to convert the photon flux into the photon absorption rate (in a unit of s^{-1}).

$$\Sigma_{a,\,Gain}^{Pump} = \sigma_{a,\,Gain}^{Pump} V_0 n_{T,Gain}, \quad (3.10)$$

$$P_{th} = I_{th} \Sigma_{a,\,gain}^{Pump} \quad (3.11)$$

$S_{a,Gain}$ is the total absorption cross section of the gain molecules inside the microlaser at the pump wavelength. P_{th} is the interaction rate between the pump photons and the entire gain molecules within the microlaser (or pump photon absorption rate at the lasing threshold). According to the above conversion, the sensitivity of the microlaser-based method, S_{Laser}, can be defined as

$$S_{Laser} = \frac{dP_{th}}{dk} = \frac{1}{\tau_{Gain}} \frac{1}{\left(1 - \gamma_0 - \frac{k}{V_0 n_{T,Gain}}\right)^2}. \quad (3.12)$$

From (3.12), we can see that when k (the analyte number) is small as compared to the total number of gain molecules, which is on the order of 10^{10} for a microlaser (for a dye laser with concentration on the order of 0.1 M and diameter of 5 μm), S_{Laser} remains a constant. However, when the ratio between the number of analytes and the total number of the gain molecules approaches g_0, S_{Laser} starts to increase significantly with respect to k.

C. Comparison Between Fluorescence- and Microlaser-Based Methods

Based on (3.5) and (3.12), the sensitivity ratio, R_{Sens} between the microlaser-based and fluorescence-based methods can be expressed as:

$$R_{Sens} = \frac{S_{Laser}}{S_{Fl}} = \frac{1}{R_{Collect}} \frac{1}{Q_e} \frac{\tau_{Fl}}{\tau_{Gain}} \frac{1 + \frac{I_{p,Fl}}{I_{sat,Fl}}}{\frac{I_{p,Fl}}{I_{sat,Fl}}} \frac{1}{\left(1 - \gamma_0 - \frac{k}{V_0 n_{T,Gain}}\right)^2}. \quad (3.13)$$

For a numerical comparison, we use the values in Table I, and obtain:

$$R_{Sens} = \frac{1}{1.25 \times 10^{-6}} \frac{1}{\left(1 - 0.05 - \frac{k}{6 \times 10^{10}}\right)^2}. \quad (3.14)$$

When $k << 10^{10}$, $R_{Sens} \sim 10^6$, meaning that the microlaser-based method is much better than the fluorescence-based method in examining and differentiating the analyte number (k).

TABLE I
PARAMETERS AND THEIR VALUES USED IN (3.14)

Parameter	Value	Parameter	Value
$R_{Collect}$	0.5	Q_e	1
t_{Fl}	10^{-8} s	$s_{a,Fl}$	10^{-16} cm^2
I_p	1 W cm^{-2} = 2.77 x 10^{21} m^{-2}s^{-1} (Note 1)	t_{Gain}	10^{-8} s
g_0	0.05 (Note 2)	V_0	10^{-15} m^3 (Note 3)
$n_{T,Gain}$	0.1 mol L^{-1} = 6x10^{25} m^{-3} (Note 4)	b	6x10^{11}
α	6x10^{11}		

Note 1: At wavelength of 550 nm.
Note 2: Typical value for a dye-based microlaser.
Note 3: A 10 mm x 10 mm x 10 mm cubic microlaser.
Note 4: Typical dye doping concentration (or density) in a microlaser.

Note that in all the above discussions, we have assumed that the absorption of the excitation light, $I_{p,Fl}$, in the fluorescence-based method is linear with respect to the analyte concentration (or fluorophore concentration). That is, the optical absorption of the excitation light follows the Beer-Lambert law. However, the reality is that when k is large (so is the analyte/fluorophore concentration), the Beer-Lambert law breaks down. As a result, the increase in the fluorescence signal becomes sub-linear with respect to the increase in the analyte. Mathematically, (3.3) should be changed to

$$P_{Fl} = \frac{Q_e}{\tau_{Fl}} \frac{\frac{I_{p,FL}}{I_{sat,Fl}}}{1+\frac{I_{p,FL}}{I_{sat,Fl}}} \frac{k}{1+\alpha k}, \tag{3.15}$$

where a is a parameter that accounts for the non-linearity of optical absorption at a high k. At a low k, (3.15) is reduced to (3.3). When k is very large, P_{Fl} increases sub-linearly. The sensitivity described in (3.5) becomes

$$S_{Fl} = \frac{Q_e}{\tau_{Fl}} \frac{\frac{I_{p,FL}}{I_{sat,Fl}}}{1+\frac{I_{p,FL}}{I_{sat,Fl}}} \frac{1}{(1+\alpha k)^2}. \tag{3.16}$$

Thus, the sensitivity, S_{Fl} in (3.5), is no longer constant and it decreases with respect to k.

Similarly, for the microlaser-based method, when the number of analytes is high, (3.7) should become

$$\gamma = \gamma_0 + X \frac{1}{V_0} \frac{k}{1+\beta k}, \tag{3.17}$$

where b is a parameter that accounts for the non-linearity of optical absorption of the quenchers at a large k (or a large number of quenchers). Accordingly, the sensitivity described in (3.12)

$$S_{Laser} = \frac{1}{\tau_{Gain}} \frac{1}{\left(1-\gamma_0-\frac{k}{V_0 n_{T,Gain}}\right)^2} \frac{1}{(1+\beta k)^2} \propto \frac{1}{(1-\varepsilon k)^2} \frac{1}{(1+\beta k)^2} \tag{3.18}$$

where

$$\varepsilon = \frac{1}{(1-\gamma_0) V_0 n_{T,Gain}}. \tag{3.19}$$

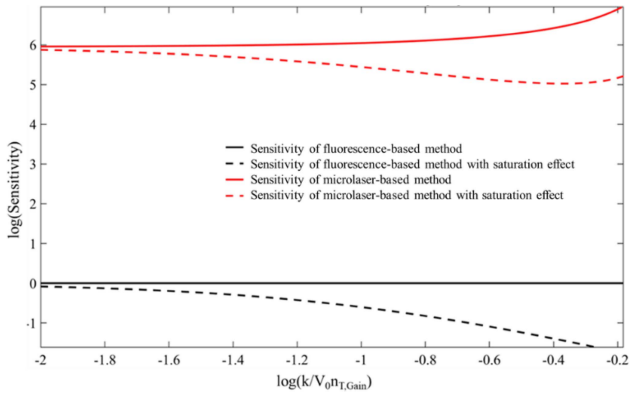

Fig. 5. An illustration of sensitivity comparison between the microlaser-based method and the fluorescence-based method. The sensitivity of the fluorescence-based method is set to be 1. The solid line shows the sensitivity of each method without considering the saturation effect. The sensitivity of the microlaser-based method is calculated using (3.4). The dashed lines show the sensitivity of each method with saturation effect. For the fluorescence-based method, the sensitivity is calculated using (3.16), whereas the sensitivity for the microlaser-based method is shown in (3.18). The saturation factor for the two methods, α and β, as shown in (3.16) and (3.18), are both set to be $10V_0 n_{T,Gain}$.

Thus, the first term in (3.18) counteracts the second term to mitigate the sensitivity-decreasing effect at a large k.

To further show the high sensitivity of the microlaser-based method over conventional fluorescence-based methods, and the mitigation effect of microlaser quenching against the saturation effect (absorption), we plot the sensitivity comparison of the two methods with the numerical values we used for (3.14) in Fig. 5. The numbers used to estimate the ratio are shown in Table I. We set the sensitivity value for the fluorescence-based method without saturation effects to be 1, and the sensitivity for the microlaser-based method without saturation effect is then in the form of (3.14). For the comparison of sensitivity with saturation effect, the sensitivity for fluorescence-based value is shown in (3.16), where we set the saturation factor α to be $10V_0\, n_{T,Gain}$. For a fair comparison, we set β, the saturation effect for the microlaser-based method in (3.18), to be the same as α. Using (3.16) and (3.18), we can calculate the sensitivity of the two methods with the saturation effect. Note that for the microlaser-based method, the mitigation effect averts the sensitivity from further dropping at high analyte number (where the derivative of the sensitivity curve becomes positive).

D. Sensitivity of Sensor Ensembles

When an ensemble of fluorescence-based sensors and an ensemble of microlaser-based sensors are incubated with the same analyte of a fixed concentration, both ensembles have the same analyte distribution over their respective sensors within the ensemble. Using $N(\mu_c,\ \sigma_c)$ to represent the Gaussian distribution of analytes in both ensembles, e fluorescence signal, $P_{Fl,}$ has a Gaussian distribution denoted by $N(\mu_c^{Fl},\ \sigma_c^{Fl})$, where:

$$\mu_c^{Fl} = R_{collect} \frac{Q_e}{\tau_{Fl}} \frac{I_p \sigma_{a,Fl} \tau_{Fl}}{1+I_p \sigma_{a,Fl} \tau_{Fl}} \mu_c, \tag{3.20}$$

$$\sigma_c^{Fl} = R_{collect} \frac{Q_e}{\tau_{Fl}} \frac{I_p \sigma_{a,Fl} \tau_{Fl}}{1+I_p \sigma_{a,Fl} \tau_{Fl}} \sigma_c. \tag{3.21}$$

Similarly, the microlaser-based sensing signal, P_{th}, has a Gaussian distribution denoted by $N(\mu_c^{th},\ \sigma_c^{th})$, where:

$$\mu_c^{th} = \frac{1}{\tau_{Gain}} \frac{1}{(1-\ \gamma_0)^2}\mu_c, \tag{3.22}$$

$$\sigma_c^{th} = \frac{1}{\tau_{Gain}} \frac{1}{(1-\ \gamma_0)^2}\sigma_c. \tag{3.23}$$

Note that for simplicity, we assume that $k \ll V_0 n_{T,Gain}$, which is usually true in most cases. Equations (3.20)–(3.23) show how the distribution of analytes over the sensors is transformed to the distribution of the sensing signal. As discussed previously in Section III-C, $\frac{1}{\tau_{Gain}} \frac{1}{(1-\ \gamma_0)^2}$ is much larger than $R_{collect}\frac{Q_e}{\tau_{Fl}} \frac{I_p\sigma_{a,Fl}\tau_{Fl}}{1+I_p\sigma_{a,Fl}\tau_{Fl}}$. Therefore, the mean value and the spread of the signal distribution in the microlaser-based method is much larger than the counterparts in the fluorescence-based method, thus making the microlaser-based method much more sensitive to detect the analyte distribution within the sensor ensemble.

E. Sensitivity of Microlasers With Multiple Quenchers Per Analyte

In the previous sensitivity comparison sections, we set the number of quenchers to be equal to the analyte number (i.e., $N_q = k$) for the sake of fair comparison. We set

$$\frac{dP_{th}}{dk} = \frac{dP_{th}}{dN_q}\ . \tag{3.24}$$

For the enzyme method, using P_{th}^{enzyme} to denote the sensing signal, we have:

$$S_{Laser}^{Enzyme} = \frac{dP_{th}^{Enzyme}}{dk}\ = \frac{dP_{th}^{Enzyme}}{dN_q}\ \frac{dN_q}{dk}. \tag{3.25}$$

We further use C_{amp} to represent the number of quenchers produced by one analyte, i.e.,

$$C_{amp} = \frac{dN_q}{dk}. \tag{3.26}$$

Therefore, the sensitivity of the microlaser-based method is increased by a factor of C_{amp} when enzyme catalyzed reaction is employed, i.e.,

$$S_{Laser}^{Enzyme} = C_{amp}\ S_{Laser}. \tag{3.27}$$

V. Detection Limit

The detection limit of the system for a specific analyte is the minimum analyte concentration that produces a measurable change in the microlaser ensemble. The measurable change in the microlaser ensemble is a change in the lasing threshold distribution that is not masked by the system noise. We consider the major system noise to be the inhomogeneity of the microlaser ensemble, meaning that the microlasers in the ensemble have minor differences in lasing thresholds, which may be caused by factors such as differences in gain medium densities during doping or other fabrication processes. We use a Gaussian distribution to approximate the lasing threshold distribution. This means that when there are no analytes in the system, we can still measure a lasing fraction similar to (2.2):

$$Lf(i) = \phi_{cumu}\left(k\ =\ 0; \mu_0, \sigma_0\right). \tag{4.1}$$

μ_0 and σ_0 are the parameters describing the lasing threshold distribution when no analyte is present. In this picture, μ_0 remains the same as the noise-free case, since the mean lasing threshold is not changed with the noise source, while σ_0 represents a broadening of the lasing threshold distribution when no analyte is present.

At the detection limit C_0, the mean captured molecule number for the microlaser ensemble is k_0. The new lasing fraction is then:

$$Lf(i) = \phi_{cumu}\left(k_i; \mu\ = k_0\ , \sigma\right). \tag{4.2}$$

Here, μ and σ are the Gaussian parameters for the microlaser ensemble after capturing molecules. Since the two factors that lead to a lasing threshold distribution are independent (inherent gain medium distribution differences and external bonded molecule number differences), for this change of the lasing threshold distribution to be measurable, we need to have:

$$k_0 - \mu_0 > \sigma_0. \tag{4.3}$$

As indicated in (2.2), $\mu_0\ \sim\ 0$. Therefore, the detection limit for the system is $k_0 = \sigma_0$. This indicates that a microlaser ensemble with higher homogeneity will have a lower detection limit. For the test sample, the detection limit is then the analyte concentration C_0 that leads to a mean captured molecule number of k_0. The specific value for C_0 depends on multiple factors such as the affinity of analytes to the capture antibodies.

VI. Discussion and Conclusion

When estimating the distribution of analytes, we used a Gaussian distribution instead of a Poisson distribution. In Methods and Results, we justified the approximation from a Poisson distribution to a Gaussian distribution when the mean of the Poisson distribution is large. Here, we give a few more reasons for using a Gaussian distribution. First, in the analyte binding step, the binding events are not independent, since there are limited binding sites on the microlasers. For a microlaser, the more analytes it has captured, the fewer vacant binding sites remain, and therefore a smaller probability for the next binding event. Using a Gaussian distribution can fit the true analyte distribution better since it has two free parameters, and the mean and the variance are independent. Even if the depletion effect mentioned earlier is weak in some cases, and the true analyte distribution is Poisson-like, using a Gaussian distribution to fit the true analyte distribution does not introduce extra fitting errors for the fitted mean analyte number. This is because when we use a Gaussian distribution to fit a Poisson distribution using maximum likelihood, the mean and variance of the Gaussian distribution will be the same as the Poisson distribution. Therefore, using a Gaussian distribution allows better fitting to the true analyte distribution over a large range of mean analyte numbers and hence a large range of analyte concentration.

In conclusion, we presented a bioassay platform based on microlaser ensembles. We established the quantitative relationship between lasing threshold changes and the number of

captured analytes for each microlaser. We proposed a measurement scheme that employs multiple pump intensity scanning and binary lasing threshold readout (higher or lower than the pump intensity) of individual microlasers and avoids direct lasing intensity measurements. This design avoids noise arising from fluctuations in lasing intensity. We extended this model to microlaser ensembles, enabling statistical recovery of analyte distributions through lasing fraction measurements. Measuring the statistical distribution of the microlaser ensemble reduces the variance from single microlasers, thus achieving stable optical signals. Furthermore, this system also eliminates the need for precise integration time tuning or specialized weak-signal detection devices. A microlaser with a weak lasing signal that is not detected at one pump intensity will lase strongly at the next higher pump intensity and be reliably detected. By fitting the number of bright microlasers to a cumulative distribution function across multiple pump intensities, the method is robust against a small fraction of missed microlasers. Each microlaser functions as a microunit that can read out the number of captured analytes in the microunit by controlling the external pump. This gives our platform a high dynamic range over digital ELISA and its variants, whose microunits only produce binary outputs. We then showed a detection limit of the platform based on microlaser ensemble inhomogeneity. While our model demonstrated that the microlaser ensemble method is no longer bounded by the saturation problem in digital ELISA, dynamic ranges in assays are also affected by biochemical factors. Ligand-binding kinetics, non-specific binding and other effects all contribute to the eventual dynamic range and detection limit of the platform.

Altogether, our theory established microlaser ensembles as a high-potential and robust bioassay platform that can achieve a high sensitivity and a high dynamic range. With the recent developments in integrated photonics and semiconductor fabrication, we foresee that this platform can be implemented using compact, highly uniform, and low-cost microlaser ensembles, such as vertical-cavity surface-emitting laser (VCSEL) arrays.

REFERENCES

[1] D. Wild, *The Immunoassay Handbook: Theory and Applications of Ligand Binding, ELISA and Related Techniques*. Oxford, U.K.: Newnes, 2013.

[2] D. S. Hage, "Immunoassays," *Anal. Chem.*, vol. 71, no. 12, pp. 294–304, 1999.

[3] I. Surugiu, B. Danielsson, L. Ye, K. Mosbach, and K. Haupt, "Chemiluminescence imaging ELISA using an imprinted polymer as the recognition element instead of an antibody," *Anal. Chem.*, vol. 73, no. 3, pp. 487–491, 2001.

[4] M. Herrmann, T. Veres, and M. Tabrizian, "Enzymatically-generated fluorescent detection in micro-channels with internal magnetic mixing for the development of parallel microfluidic ELISA," *Lab Chip*, vol. 6, no. 4, pp. 555–560, 2006.

[5] C. Hempen and U. Karst, "Labeling strategies for bioassays," *Anal. Bioanalytical Chem.*, vol. 384, pp. 572–583, 2006.

[6] C. M. O'Donnell and S. C. Suffin, "Fluorescence Immunoassays," *Anal. Chem.*, vol. 51, no. 1, pp. 33A–40A, 1979.

[7] E. R. Goldman, I. L. Medintz, and H. Mattoussi, "Luminescent quantum dots in immunoassays," *Anal. Bioanalytical Chem.*, vol. 384, pp. 560–563, 2006.

[8] R. Thürer et al., "Potentiometric Immunoassay with quantum dot labels," *Anal. Chem.*, vol. 79, no. 13, pp. 5107–5110, 2007.

[9] Y. Lv et al., "Development of dual quantum dots-based fluorescence-linked immunosorbent assay for simultaneous detection on inflammation biomarkers," *Sensors Actuators B: Chem.*, vol. 301, 2019, Art. no. 127118.

[10] M. Helle, L. Boeije, E. de Groot, A. de Vos, and L. Aarden, "Sensitive ELISA for interleukin-6: Detection of IL-6 in biological fluids: Synovial fluids and sera," *J. Immunological Methods*, vol. 138, no. 1, pp. 47–56, 1991.

[11] J. Gratacos et al., "Serum cytokines (IL-6, TNF-α, IL-1β and IFN-γ) in Ankylosing Spondylitis: A close correlation between serum IL-6 and disease activity and severity," *Rheumatology*, vol. 33, no. 10, pp. 927–931, 1994.

[12] S. A. Khan, J. Joyce, and T. Tsuda, "Quantification of active and total transforming growth factor-β levels in serum and solid organ tissues by bioassay," *BMC Res. Notes*, vol. 5, pp. 1–9, 2012.

[13] S. Jayasena et al., "Comparison of six commercial ELISA kits for their specificity and sensitivity in detecting different major peanut allergens," *J. Agricultural Food Chem.*, vol. 63, no. 6, pp. 1849–1855, 2015.

[14] A. A. Al-Hosary, J. Ahmed, A. Nordengrahn, and M. Merza, "Assessment of the first commercial ELISA kit for the diagnosis of Theileria Annulata," *J. Parasitol. Res.*, vol. 2015, no. 1, 2015, Art. no. 787812.

[15] D. M. Rissin et al., "Single-molecule enzyme-linked immunosorbent assay detects serum proteins at subfemtomolar concentrations," *Nature Biotechnol.*, vol. 28, pp. 595–599, 2010.

[16] J. Hwang et al., "Quantitation of low abundant soluble biomarkers using high sensitivity single molecule counting technology," *Methods*, vol. 158, pp. 69–76, 2019.

[17] S. A. Byrnes et al., "Wash-free, digital immunoassay in polydisperse droplets," *Anal. Chem.*, vol. 92, pp. 3535–3543, 2020.

[18] L. Cohen et al., "Single molecule protein detection with attomolar sensitivity using droplet digital enzyme-linked immunosorbent assay," *Amer. Chem. Soc. Nano*, vol. 14, pp. 9491–9501, 2020.

[19] Y. Song et al., "A digital protein microarray for COVID-19 cytokine storm monitoring," *Lab Chip*, vol. 21, pp. 331–343, 2021.

[20] Z. Gao et al., "Machine-learning-assisted microfluidic nanoplasmonic digital immunoassay for cytokine storm profiling in COVID-19 patients," *Amer. Chem. Soc. Nano*, vol. 15, pp. 18023–18036, 2021.

[21] C. Wu, T. J. Dougan, and D. R. Walt, "High-throughput, high-multiplex digital protein detection with attomolar sensitivity," *Amer. Chem. Soc. Nano*, vol. 16, pp. 1025–1035, 2022.

[22] C. Chen et al., "Microfluidic digital immunoassay for point-of-care detection of NT-proBNP from whole blood," *Anal. Chem.*, vol. 96, pp. 10569–10576, 2024.

[23] Y. Zhang and H. Noji, "Digital bioassays: Theory, applications, and perspectives," *Anal. Chem.*, vol. 89, no. 1, pp. 92–101, 2017.

[24] J. Zhang et al., "Improving the accuracy, robustness, and dynamic range of digital bead assays," *Anal. Chem.*, vol. 95, pp. 8613–8620, 2023.

[25] M. Aas, Q. Chen, A. Jonáš, A. Kiraz, and X. Fan, "Optofluidic FRET lasers and their applications in novel photonic devices and biochemical sensing," *IEEE J. Sel. Topics Quantum Electron.*, vol. 22, no. 4, Jul./Aug. 2016, Art. no. 7000215.

[26] S. Lacey et al., "Versatile opto-fluidic ring resonator lasers with ultra-low threshold," *Opt. Exp.*, vol. 15, no. 23, pp. 15523–15530, 2007.

[27] H.-J. Moon, Y.-T. Chough, and K. An, "Cylindrical microcavity laser based on the evanescent-wave-coupled gain," *Phys. Rev. Lett.*, vol. 85, no. 15, 2000, Art. no. 3161.

[28] A. E. Siegman, "Lasers," in *University Science Books*, Melville, NY,USA: 1986.

[29] W. Wu, Y. Cao, X. Tan, and X. Fan, "Sensitive bioassay with an ultra-large dynamic range via microlaser ensemble quenching," *ACS Sensors*, vol. 10, pp. 6436–6445. 2025.

Weishu Wu received the B.S. degree in physics from Fudan University, Shanghai, China, in 2018, and the M.Sc. degree in electrical and computer engineering and the Ph.D. degree in biomedical engineering from the University of Michigan, Ann Arbor, MI, USA, in 2020 and 2025, respectively. He is currently a Research Fellow with the University of Michigan.

Xudong Fan received the B.S. and M.S. degrees from Peking University, Beijing, China, in 1991 and 1994, respectively, and the Ph.D. degree in physics and optics from the Oregon Center for Optics, University of Oregon, Eugene, OR, USA, in 2000. Between 2000 and 2004, he was a Project Leader with 3 M Company. In 2004, he joined the Department of Biological Engineering, University of Missouri, Columbia, MO, USA, as an Assistant Professor and was promoted to Associate Professor in 2009. In 2010, he joined the Biomedical Engineering Department, University of Michigan, Ann Arbor, MI, USA and was promoted to Professor in 2014. His research interests include photonic bio/chemical sensors, micro/nano-fluidics, gas sensors, portable gas chromatography, and nanophotonics for disease diagnostics and bio/chemical molecule analysis. Dr. Fan is a fellow of Optical Society of America (now Optica), SPIE, and Royal Society of Chemistry.